IAC-14-A6.P.31

CONTINUITY EQUATION APPROACH FOR THE ANALYSIS OF THE COLLISION RISK DUE TO SPACE DEBRIS CLOUDS GENERATED BY A FRAGMENTATION EVENT

Francesca Letizia
Astronautics Research Group, University of Southampton, United Kingdom, f.letizia@soton.ac.uk

Camilla Colombo
Department of Aerospace Science and Technology, Politecnico di Milano, Italy, camilla.colombo@polimi.it

Hugh G. Lewis
Astronautics Research Group, University of Southampton, United Kingdom, H.G.Lewis@soton.ac.uk

As the debris population increases, the probability of collisions in space grows. Even a collision involving small objects may produce thousands of fragments due to high orbital velocity and the high energy released in the collision. The propagation of the trajectories of all the objects would be prohibitive in terms of computational time, so simplified models have been proposed to describe the consequences of a collision with a reasonable computational effort. In this work, the consequences of a collision are simulated focusing on the description of the behaviour of the fragments cloud as a whole and applying the continuity equation. A debris cloud in Low Earth Orbit (LEO) is modelled as a fluid, whose spatial density varies with time, under the effect of the Earth's gravity and atmospheric drag. Introducing some simplifying assumptions, such as an exponential model of the atmosphere and the hypothesis of limited eccentricity for the fragments' orbits, an analytical expression for the cloud density evolution in time is derived. This novel approach enables the analysis of a large number of potential fragmentation scenarios that would be time-limited with current numerical methods that rely on the integration of the all the fragment trajectories through semi-analytical expression of the dynamics. Moreover, compared to the approaches where only some representative objects are propagated, this method operates directly on the objects spatial density, which is then used to compute the collision probability.Results will be shown considering different collisions scenarios, considering the fragmentation of satellites at different altitudes and inclinations. In this way, it is possible to identify orbiting objects that, in case of fragmentation, are more likely to generate a debris cloud that can create a hazard to reference operative satellites in LEO.

I. INTRODUCTION

Past space missions have left millions of non-operative objects in orbit and also current missions, despite mitigation measures, continue to increase the number of debris objects because, quoting Chobotov [1], "space debris is a *self-perpetuating issue* as any new space mission generates new objects". Currently, the focus is mostly on the largest objects of the debris population, meaning the 22 000 objects larger than 10 cm that are constantly tracked from the Earth to avoid operational spacecraft to collide with them. This object size has also been the main scope for the evolutionary studies on the space debris population, which analyses the long term response to the variation of some parameters such as launch routines, percentage of compliance to regulations, implementation of active removal missions.

However, White and Lewis [2] showed that the effect of remediation measures is not the same on the population of objects larger than 10 cm and on the one of objects between 5 and 10 cm as the latter may still increase even when the former is supposed to decrease. In other words, focussing only on the large fragments may lead to an underestimation of the collision risk. In fact, also *small* fragments can pose a relevant hazard to other spacecraft. In particular, objects larger than 1 mm are yet able to interfere with operational spacecraft causing anomalies and objects larger than 1 cm can even destroy a satellite in case of collision [3].

The models currently employed to study the debris evolution cannot be simply *extended* to consider more fragments in their analysis: the number of objects larger than 1 cm is around 500 000 and more than ten millions objects larger than 1 mm are supposed to be in orbit around the Earth. These numbers are too large to consider feasible a piece-by-piece analysis of the debris population as the resulting computational time would be prohibitive. For this reason, some existing models [4] sample the small fragments and define some representative objects, which are the only ones to be propagated. The re-

sult of the propagation is then used to compute the resulting collision probability, so the representative objects need to be re-converted into a distribution of small fragments or in a value of fragment density.

This work discusses instead the applicability of a novel method, where the small fragments are modelled in terms of their spatial density. This approach presents two main advantages:

- the method operates directly on the spatial density, which can be used to compute the contribution to the collision probability due to the small fragments,
- the formulation in terms of spatial density admits an analytical solution for the evolution of the fragment density, if only the effect of drag is considered.

In the following, the method will be briefly outlined in Sec. II, while an analysis is presented in Sec. III-V for what concerns the most recent innovations to the proposed approach. Finally, Sec. VI discusses some possible applications of the method.

II. METHOD OVERVIEW

An analytical approach to space debris population in Low Earth Orbit (LEO) was originally proposed by McInnes[5]: assuming that the space debris population has a spherical distribution around the Earth and considering only the effect of drag, the application of the continuity equation to the system allows obtaining an explicit expression for the debris density in time. Here, instead, this approach is used to model a single fragmentation event and assess its impact in terms of fragment spatial density and change in the collision probability for a target spacecraft.

For this purpose, McInnes' analytical propagation[5] is incorporated as one of the building blocks (Fig. 1) required to model a fragmentation event from its beginning (the breakup) to the long term evolution. The resulting method, CiELO[6] is here briefly summarised.

Compared to the previous version of the method[6], a fifth block is added to the diagram, so that now given the trajectory of a target spacecraft, CiELO can compute the collision probability due to the fragment cloud. In this section, a short description of each block in Fig. 1 is provided, whereas a detailed description of the block 3 *Position fitting* is given in Sec. III and Sec. IV and of block 5 *Collision probability* in Sec. V. For further details on the overall method the reader can refer to Ref. [6].

II.I. Breakup model

The generation of the fragments due to a collision or an explosion requires a breakup model able to describe how the energy of the fragmentation event is distributed among the fragments and to define their characteristics (e.g., mass, size). In this work, the NASA breakup model[7,8] is used considering only the fragment with size between 1 mm and 8 cm. The results in the following refer all to non-catastrophic collisions, but the analytical method is able to deal also with the other kinds of fragmentation events (i.e., catastrophic collisions and explosions).

II.II. Numerical propagation

Once the fragments are generated, their orbital parameters are numerically propagated to model the short initial phase of the cloud evolution when the Earth's oblateness has the dominant effect[9,10]. The numerical propagator used here is based on Gauss' equations and each fragment trajectory is considered separately. The numerical propagation models the secular effect of the Earth's oblateness[11], considering the J_2 term only, and the effect of the atmospheric drag, considering the average variation of the parameters along one orbit as obtained by King-Hele[12]. This numerical propagator is also used as a baseline for the validation of the long term analytical propagation.

The numerical propagation is stopped once the fragments are spread and form a band around the Earth. From this moment, the problem can be studied with the analytical method proposed by McInnes[5], which assumes drag to be the driver of the evolution and a spherical symmetry for the system. The time required to form a band around the Earth can be estimated through Ashenberg's theory[13] : it provides a stop criterion that does not require any continuous check on the fragment propagation, which can therefore be parallelised, reducing the computational time.

Work is ongoing to model also this initial phase through the same approach used in block 4 *Analytical propagation*[14]. This would further reduce the computation time of the CiELO method and make it completely independent from the number of fragments in the cloud.

II.III. Position fitting

As anticipated in the description of the previous block, once the fragments form a band around the Earth, it is possible to change the point of view from the single fragments to the whole cloud. This requires to convert the information on the position of all the fragments into a continuous density function. Different approaches are possible here, depending on the use of distribution func-

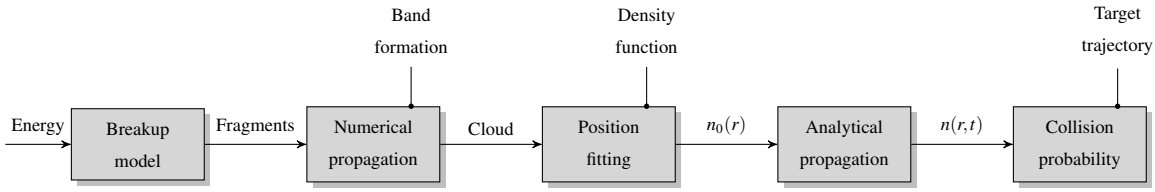

Fig. 1: CiELO building blocks.

tions[15] or fitting functions[6], which appears to give the best results. A detailed discussion on the functions used to fit the initial distribution of fragments $n_0(r)$ is provided in Sec. III.

II.IV. Analytical propagation

The long term evolution of the cloud is obtained by applying the continuity equation to model the effect of the atmospheric drag[5]. Using n to indicate the fragment density, the continuity equation is written as

$$\frac{\partial n(r,t)}{\partial t} + \nabla \bullet \mathbf{f} = 0, \qquad [1]$$

where $\mathbf{f}$ is the vector field that models drag.

Assuming that the system can be considered spherically symmetrical, it can be studied through only one coordinate, the distance r. Therefore, $\mathbf{f}$ has only one component, f_r with

$$f_r = v_r n(r,t) \qquad [2]$$

and v_r is the radial velocity due to drag[5]

$$v_r = -\varepsilon\sqrt{r}\exp\left(-\frac{r-R_H}{H}\right) \qquad [3]$$

where ε collects all the terms that do not depend on the distance r

$$\varepsilon = \sqrt{\mu}\frac{c_D A}{M}\rho_H$$

such as the gravitational constant μ, the drag coefficient c_D, the fragment cross area A and mass M. ρ_H, together with R_H and H, derives instead from the exponential model of the atmosphere

$$\rho = \rho_H \exp\left(-\frac{r-R_H}{H}\right)$$

used within the analytical approach.

It should be observed that Eq. 3 is rigorously valid only for circular orbits, so the analytical method assumes that all the fragments are on quasi-circular orbits. This means that the method can be applied only to model fragmentations on circular orbits, which are, in any case, where the vast majority of catalogued objects can be found[16]. In addition, the hypothesis of circular orbits also limits the altitudes where the method is applicable because at low altitude (< 800 km) eccentricity has large impact on the accuracy of the propagation[6]. Despite this constrain, the analytical method can be still applied to study the regions in LEO with the highest debris density as they are around and above 800 km[16].

Substituting Eq. 2 in the continuity equation (Eq. 1) and applying the method of characteristics to transform the partial differential equation into a system of ordinary differential equations, an explicit expression for the fragment spatial density is found

$$n(r,t) = n_0(r_i)\frac{r_i^2 v_r(r_i)}{r^2 v_r(r)} \qquad [4]$$

where n_0 is the initial distribution obtained from the block 3 *Position fitting* and r_i is a function

$$r_i = g(r,t)$$

that derives from inverting the expression of the characteristics at the *initial* time $t = 0$. For further information on the mathematical details the interested reader can refer to Refs.[6,14]. To improve the accuracy, the fragments in the cloud are classified considering their area-to-mass ratio (A/M); for this application, a discretisation in $N_{A/M} = 10$ bins of A/M is used as it was shown that this number is optimal in the trade-off between the increase of the computational time and the reduction of the method error[6]. For each value of A/M a *partial* density n_j is defined and Eq. 4 is applied to obtain each n_j; the total density is simply obtained by summing all the n_j

$$n(r,t) = \sum_{j=1}^{N_{A/M}} n_j(r,t) = \sum_{j=1}^{N_{A/M}} n_{0,j}(r_{i,j})\frac{r_{i,j}^2 v_{r,j}(r_{i,j})}{r^2 v_{r,j}(r)}.$$

Through to Eq. 4, the value of the density at a certain altitude and at a certain instant of time is immediately known. This can be used, for example, to produce a plot such as in Fig. 2. The figure shows the evolution of a fragment cloud obtained by applying the analytical approach. The cloud is generated by a non-catastrophic collision (energy equal to 100 kJ) on a planar circular orbit at 800 km and it is formed by 3000 fragments larger than 1 mm. The time on the y-axis is measured from the band formation, when it is possible to identify a distinct peak in the cloud density at the altitude of the breakup. With time, drag reduces the value of the density peak and the number of fragments at low altitudes; the density at

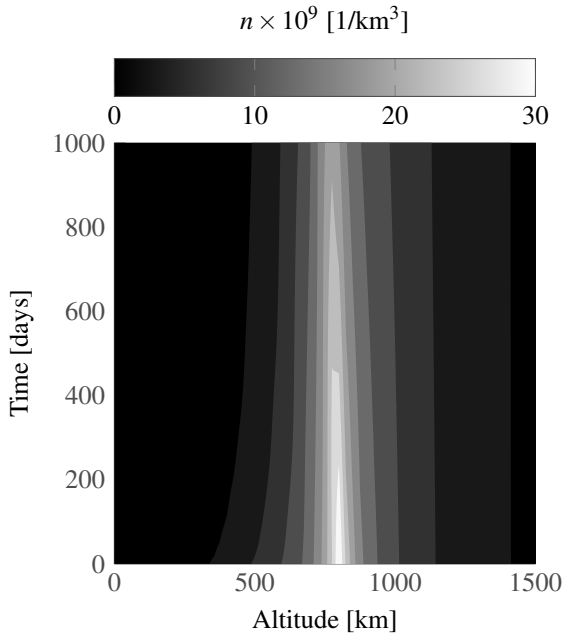

Fig. 2: Visualisation of cloud density evolution in altitude and time for a fragmentation at 800 km on a planar orbit.

high altitudes is, instead, almost unchanged. This figure is effective in showing the variation with time of the altitude range affected by the fragmentation and gives an immediate idea on the persistence of the fragments.

The use of the analytical approach for this analysis allows reducing the computational time to 10% of the time required by the full numerical propagation of the fragments trajectories (13 s against 143 s on a PC with 8 CPUs at 3.40 GHz).

II.V. Collision probability

Once the cloud density at any time is known, it is possible to evaluate its impact on the collision probability for a spacecraft that crosses the cloud. The computation of the collision probability, as explained in detail in Sec. V, is based on the average number of collisions N in an interval of time. This number is then used to obtain the cumulative collision probability for the target spacecraft

$$p_c(t) = 1 - \exp N(t_0, t) \qquad [5]$$

following the common analogy with the kinetic gas theory[9,17].

Thanks to the reduced computational time, this approach can be applied to study the collision probability in many different scenarios, enabling extended analysis on the contribution of small fragments to the collision risk and suggesting new tests to identify the most dangerous objects in the catalogued population.

III. FRAGMENT SPATIAL DENSITY

In the previous version of the method, the expression for the initial density was obtained by applying the following expression

$$n_\nu(\nu) = \frac{(1+e)^2}{(1+e\cos\nu)} \qquad [6]$$

originally proposed by McInnes and Colombo[18] to describe the probability of finding an object at a certain true anomaly ν along a given orbit. This expression has the advantage of a clear interpretation based only on the orbital mechanics, but it was found to be less accurate in describing the initial condition than the formulations by Kessler[19] and Sykes[20], both derived from the work of Öpik[21].

These two formulations are identical and express the probability of finding, at a certain distance from the central body r and a certain latitude β, a particle knowing its orbital parameters a, e, i and assuming that the distribution of the other parameters ω, Ω, ν can be considered random. These expressions depend only on geometry, so they have been applied to different problems related to space debris[17,22], the design of disposal trajectories[23], but also asteroids[20] and Jupiter's outer moons[19]. Moreover, the dependence on the distance and on the latitude can be studied separately, which is particularly useful in the current application as the evolution of the two parameters occurs with different time scales and drivers.

For this reason, in this part only the expression as a function of the distance r is analysed, whereas the role of latitude is discussed in Sec. IV.

According to Kessler's[19] and Sykes'[20] expressions, the spatial density in a particle band can be expressed as

$$S(r, \beta) = s(r) f(\beta) \qquad [7]$$

where

$$s(r) = \frac{1}{4\pi r a} \frac{1}{\sqrt{e^2 - \left(\frac{r}{a} - 1\right)^2}} \qquad [8]$$

$$f(\beta) = \frac{2}{\pi} \frac{1}{\sqrt{\cos^2\beta - \cos^2 i}}, \qquad [9]$$

so Eq. 8 is the equation used to build the initial condition.

As in the previous version of the model[6], the dispersion of the orbital parameters a, e among the fragments should be considered. This means that Eq. 8 cannot be used directly to describe the density of the cloud using from the initial value of a, e of the orbit where the fragmentation occurred, but it should be applied to each fragment to take into account how the energy is distributed among them; the total density is then obtained by simply

summing the contribution of each fragment. In the following, the comparison between the two formulation is shown and the validation of the analytical method with the expression in Eq. 8 is carried out.

III.I. Comparison between the density expressions

The two expressions for the density, Eq. 6 and Eq. 8, were initially tested considering their accuracy in modelling the initial density profile, which is the distribution of the fragments at the band formation. This was done both on single runs of the NASA breakup model and on an average distribution obtained with ten runs of the breakup model.

Fig. 3 shows this last test performed considering ten different runs of the NASA breakup model for a non-catastrophic collision with energy equal to 100 kJ, occurring on a circular planar orbit at 800 km. The grey bars represent the average distribution of fragments; the grey lines the profiles obtained applying Eq. 6 to each run of the breakup model and the black lines the resulting profiles applying instead Eq. 8.

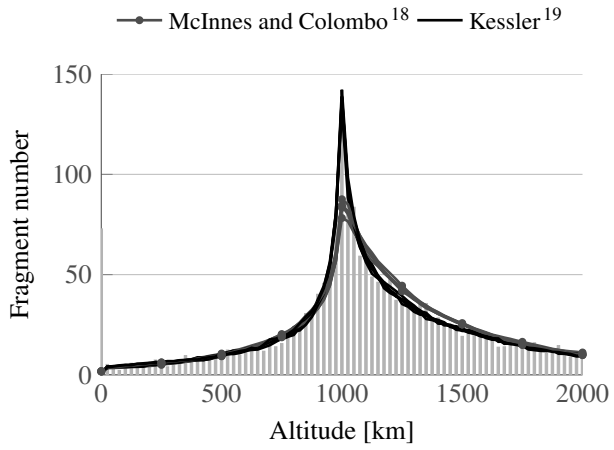

Fig. 3: Comparison between the density expressions to represent the average fragment spatial distribution at the band formation obtained with ten runs of the breakup model.

The comparison is here expressed through the number of fragments in an altitude shell of width equal to 25 km; Eq. 6 expresses its result directly in this term, whereas Eq. 8 provides a spatial density, so its output need to be multiplied by the volume of the spherical shell. From Fig. 3 it is possible to observe how both the expression capture the general shape of the distribution, but Eq. 8 is more effective in representing the peak in the distribution. Moreover, Eq. 8 shows lower variability among the different runs and this is very important because it confirms, as already observed[6], that the results obtained with the analytical method have a limited dependence on the specific run of the breakup model used to model a fragmentation. In fact, the density curves built from Eq. 6 and Eq. 8 represent an average spatial distribution that in the case of the numerical propagation can be build by a Monte Carlo approach to the breakup model. Similar results were obtained for different values of altitude and inclination.

III.II. Validation of the density expressions

Once the validity of using Eq. 8 was proven, the analytical method was validated following the same approach used in a previous work[6] based on Eq. 6. The validation compares the result of the analytical propagation with the density profile built starting from the data obtained with the numerical propagation. Here it is important to highlight that the comparison is done applying to the numerical data the same equations used to build the initial condition in order to focus the attention on the error due to the propagation only and not the components of error due to the density function in itself (Eq. 6 or Eq. 8) or the lack of Monte Carlo runs for the numerical propagation.

The result of the validation is shown in Fig. 4, where the curve indicates the relative error on the total number of fragments predicted to be still in orbit after 1000 days from the band formation.

As already found for Eq. 6[6], the accuracy of the method is good only for altitudes equal or larger than 800 km, where the error is always lower than 15%, whereas at lower altitudes the effect of eccentricity should be considered to improve the results[14].

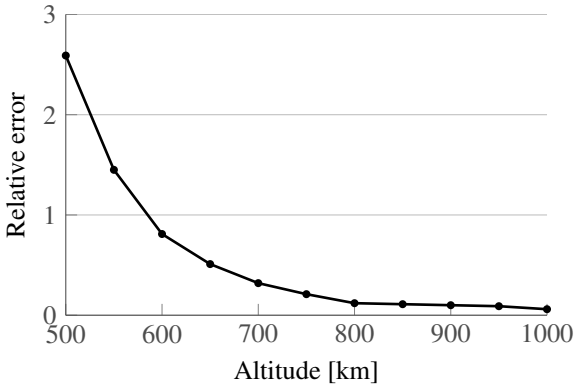

Fig. 4: Relative error of the analytical model using Eq. 8 at different altitudes.

Finally, the two definitions for the initial density were compared in different instants of time, taking as a common reference the distribution obtained from the numerical propagation as shown in Fig. 5. Observe that here

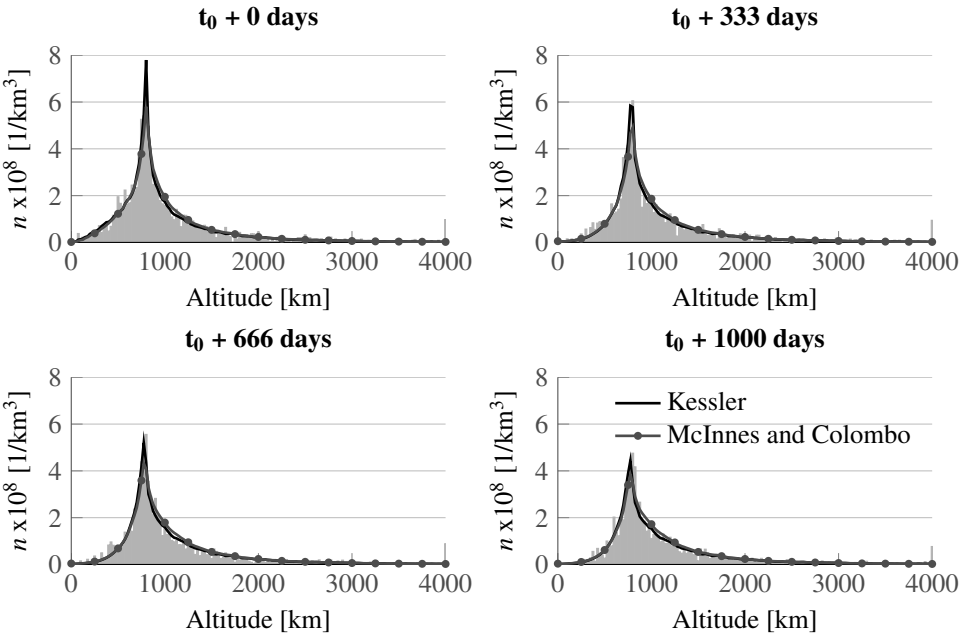

Fig. 5: Fragment spatial density for a fragmentation at 800 km, on a planar orbit. The band is formed after $t_0 = 95$ days and the time on top of each plot is measured from that moment. The grey bars represent the distribution of fragments obtained with the numerical propagation, the black line represents the result of the analytical propagation using Eq. 8 and grey one using Eq. 6.

the numerical propagation is done starting from only one run of the NASA breakup model and this explains why there is larger difference between the histograms and the continuous curves compared to the average distribution in Fig. 3. Fig. 5 also shows clearly that while the value of the relative error may seem large (around 20%) the curves actually give a good representation of the fragment distribution. For this reason, future work will perform the validation of the method using an average fragment distribution starting from multiple runs of the breakup model to obtain a more precise estimation of the method accuracy.

More in detail, Fig. 5 refers to the propagation of a cloud of fragments generated by a non-catastrophic collision with energy equal to 100 kJ, occurring on a circular planar orbit at 800 km. Also in this case, the curve built from Eq. 8 appears more effective in capturing the peak. This observation can be once more generalised to other altitudes as shown in Fig. 6. The solid line, similarly to Fig. 4, indicates the relative error on the total number of fragments after 1000 days of propagation, this time measured comparing the density profile directly to the numerical distribution. The dashed line, instead, indicates the relative error on the peak of the fragment distribution, again after 1000 days from the band formation. The relative error on the total number is similar for both the expressions of density; on the other hand, Eq. 8, in black, shows a remarkable improvement in the description of the peak.

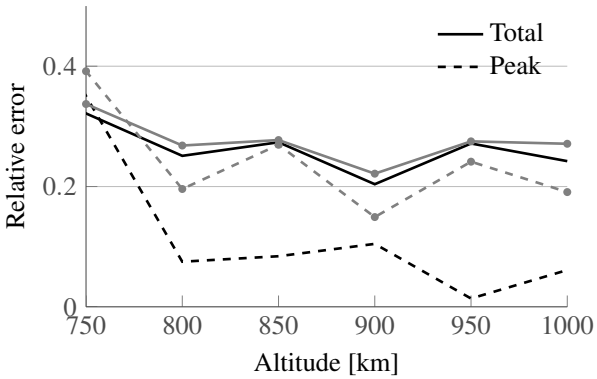

Fig. 6: Relative error of the analytical model at different altitudes using Eq. 8 in black and using Eq. 6 in grey.

IV. THE DEPENDENCE ON LATITUDE

As stated in Sec. III, the correct representation of the cloud spatial density requires to consider also the distribution in latitude. However, in this work a constant distribution in latitude is assumed, similarly to what already done in [22]. This is done because the purpose of this method is to study the long term (i.e., years) effect of a fragmentation, whereas the longitude of a target spacecraft crossing the cloud evolves in a much shorter time

scale (i.e., hours). Following correctly the target latitude would require very short time step for the integration, vanishing or reducing the advantage of having a fast propagator for the fragment cloud.

However, it is important to remark that the analytical method is able to deal also with the distribution in latitude. In fact, applying the general solution for a 2D formulation of a continuity equation problem[14] to the current application, the expression for the density can be written as

$$\tilde{n}(r,\beta,t) = \tilde{n}_0(r_i,\beta_i)\frac{v_r(r_i,\beta_i)v_\beta(r_i,\beta_i)}{v_r(r,\beta)v_\beta(r,\beta)} \qquad [10]$$

where $\tilde{n}_0$ is the initial distribution, r_i, β_i are functions obtained by inverting the characteristic lines at initial time $t = 0$, v_r, v_β are respectively the expression of dr/dt and $d\beta/dt$ due to the effect modelled by the continuity equation, i.e., drag. Therefore in this case, where the effect of draf on quasi-circular orbits is considered,

$$\frac{dr}{dt} = -\varepsilon\sqrt{R_H}\exp\left(\frac{r-R_H}{H}\right) \qquad [11]$$

$$\frac{d\beta}{dt} = 0 \qquad [12]$$

meaning that v_r depends only on r and the distribution in latitude is not directly affected by drag. As a result, Eq. 10 can be written as

$$\tilde{n} = \tilde{n}_0(r_i,\beta)\frac{v_r(r_i)}{v_r(r)}. \qquad [13]$$

The expression for $\tilde{n}_0(r_i,\beta_i)$ is simply given by Kessler[19] and Sykes[20], so using the expressions in Sec. III,

$$\tilde{n}_0(r_i,\beta_i) = S(r_i,\beta) = s(r_i)f(\beta) \qquad [14]$$

and finally

$$\tilde{n}(r,\beta,t) = f(\beta)\frac{s(r_i)v_r(r_i)}{v_r(r)}. \qquad [15]$$

Similarly to what is done for $s(r)$, $f(\beta)$ can be built at the band formation applying Eq. 9 to all fragments and summing their contribution.

In this work, as explained before, the choice was not to follow in detail the evolution of the target latitude: what is relevant for the study is knowing if the target spacecraft is inside of outside the fragment band (Fig. 7);

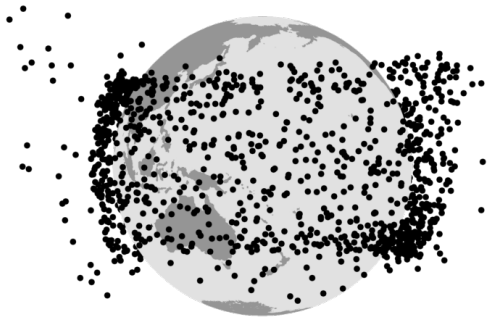

Fig. 7: Representation of the band formed by the fragments two months after the breakup. The fragments are not in scale.

if it is inside, an average value of the fragment density is used, which depends only on the distance and not on the latitude.

The average density value can be found computing the integral average of $f(\beta)$ on its domain

$$\begin{aligned}\bar{f} &= \int_{-\beta_{\max}}^{\beta_{\max}} f(\beta)\,\mathrm{d}\beta \\ &= \int_{-\beta_{\max}}^{\beta_{\max}} \frac{2}{\pi}\frac{1}{\sqrt{\cos^2\beta - \cos^2\beta_{\max}}}\,\mathrm{d}\beta\end{aligned} \qquad [16]$$

where $\beta_{\max}$ is the maximum latitude covered by the band. This integral can be solved using the non-diverging expression for f proposed by Kessler[19] and so

$$\bar{f} = \frac{1}{\sin\beta_{\max}}. \qquad [17]$$

Another way to obtain this value is to consider the geometry of the problem.

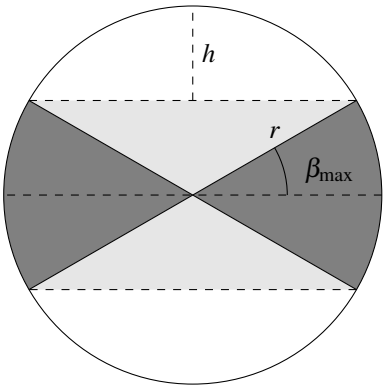

Fig. 8: Geometry of the band volume.

In fact, the volume of the band can be obtained subtracting to the volume of the sphere ($V_{\text{sph}} = \frac{4}{3}\pi r^3$) two spherical sectors whose spherical caps have height equal

to h ($V_{\text{sec}} = \frac{2}{3}\pi r^2 h$). h can be related to the angle $\beta_{\max}$ (Fig. 8)

$$h = r - r\sin(\beta_{\max})$$

so that the final expression for the band volume is

$$V_{\text{band}} = \frac{4}{3}\pi r^3 - 2\frac{2}{3}r^2 r(1-\sin\beta_{\max}) = \frac{4}{3}\pi r^3 \sin\beta_{\max} = V_{\text{sph}}\sin\beta_{\max}$$

where $\bar{f}$ can be computed again, now with the meaning of a scaling factor between the two volumes,

$$\frac{V_{\text{sph}}}{V_{\text{band}}} = \frac{1}{\sin\beta_{\max}} = \bar{f}. \quad [18]$$

The scaling factor $\bar{f}$ can be therefore applied to the spatial density $s(r)$ so that it expresses the value of the density inside the band not in the whole sphere. In equation, the fragment spatial density can be written as

$$\bar{S}(r) = \begin{cases} 0, & \text{if } |\beta| > \beta_{\max} \\ \bar{f}s(r), & \text{if } |\beta| \leq \beta_{\max}. \end{cases} \quad [19]$$

For non-planar orbits $\beta_{\max}$ is put equal to the inclination where the fragmentation occurred, following the band characterisation proposed by McKnight[9] and considering that with the current hypotheses (e.g., non-rotating atmosphere) the fragment inclination is not affected by drag and so it is constant. For planar orbits, $\beta_{\max}$ is put equal to the maximum inclination reached by the fragments because of the breakup.

V. COLLISION PROBABILITY COMPUTATION

Following Kessler's[19] approach, the collision probability for a target crossing the cloud is computed considering the average number of collisions N in a given interval of time Δt. This can be written as

$$N = F\sigma\Delta t \quad [20]$$

where F is the flux of particles and σ represents the collisional cross-sectional area. This last parameter is usually defined considering the dimensions of both the colliding objects[19], but here only the target spacecraft area A_T is considered because the fragments are much smaller than itm, so $\sigma = A_T$.

The flux F is written as

$$F = n(r,t)V \quad [21]$$

where $n(r,t)$ is the value of the spatial density obtained with propagation method explained in Section II. V is instead the average relative velocity between the targets and the fragments. To keep the formulation simple and depend only on the distance, a set of hypotheses is introduced to obtain the expression of V. Rigorously, V can be obtained from[19]

$$V^2 = V_T^2 + V_F^2 - 2V_T V_F \cos\phi \quad [22]$$

where V_T and V_F are respectively the orbital velocities of the target and of each fragment with respect to the central body; ϕ is the angle between the two vectors $\mathbf{V_T}$ and $\mathbf{V_F}$. V_T is known from the propagation of the target trajectory; V_F instead is a peace of information that is lost with the analytical propagation. However, the propagation of the fragment cloud is done under the hypothesis of quasi-circular orbits, so

$$V_F \approx V_{\text{circ}} = \sqrt{\frac{\mu}{r}}. \quad [23]$$

In this work, this approximation is extended also to the target because only targets on quasi-circular orbits are considered. Two objects on (quasi-)circular orbits can collide with an impact azimuth angle between -90° and 90°[16], with the two extreme cases resulting in the highest relative speed, which is chosen to obtain a conservative estimation. Therefore, Eq. 24 becomes

$$V^2 = 2V_{\text{circ}}^2 \rightarrow V = \sqrt{2\frac{\mu}{r}}. \quad [24]$$

The impact of this approximation was estimated by computing the actual average relative velocity between the target and the fragments in different scenarios. To clarify, the *actual* average relative velocity is computed as the average of the relative velocity between the target and each fragment in the cloud. Fig. 9 shows the result for four different cases, marked with the following naming convention

$$\mathrm{F}(h_F, i_F) - \mathrm{T}(h_T, i_T)$$

where h_F and i_F are the altitude and the inclination of the orbit where the fragmentation occurred; h_T and i_T are instead the initial altitude and inclination of the target spacecraft. Both the parent orbit of the fragmentation and the one of the target are circular.

It is possible to see that in all the cases in Fig. 9 the relative error on the velocity is around 10% and that the approximation always overestimates the real value, so that the resulting collision probability is calculate in a conservative way.

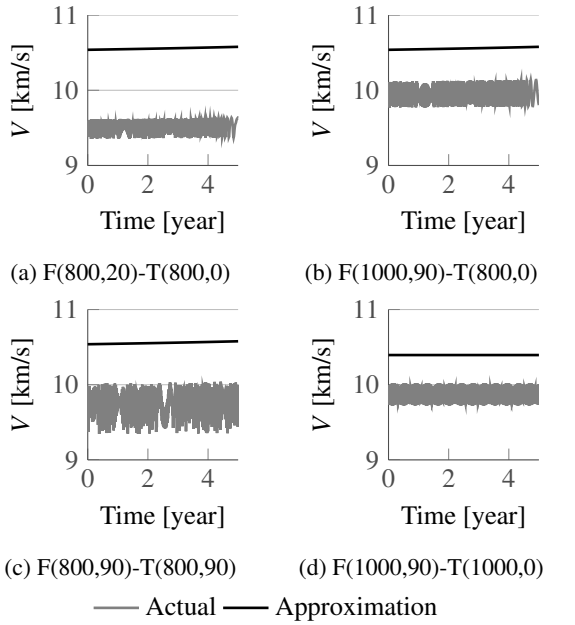

Fig. 9: Actual average relative velocity between the target and the fragments and approximated one in different scenarios.

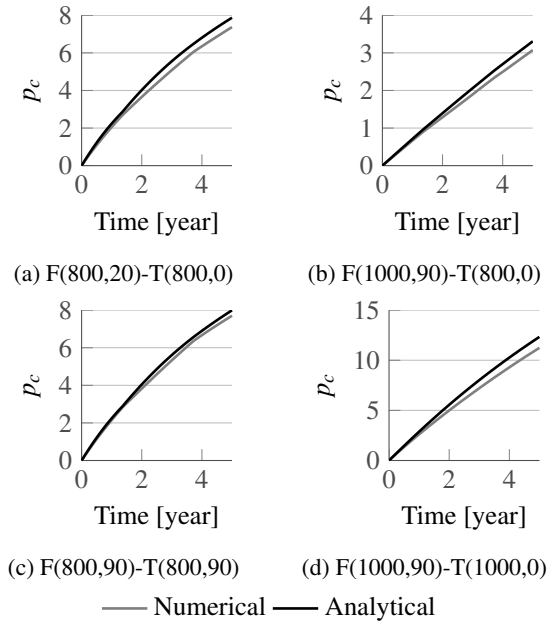

Fig. 10: Cumulative collision probability obtained with the numerical approach and with the analytical one in different scenarios.

Up to this point, the accuracy on the spatial density and on the velocity were studied separately, but it is also interesting to analyse the combined effect of the approximations. As explained in Eq. 20, the number of collisions is computed through the expression

$$N = n(r,t)V\sigma\Delta t, \qquad [25]$$

so the final test is to evaluate this expression with the values of spatial density and average relative velocity coming from the numerical propagation and the ones coming from the analytical one.

The result of this test, for the same cases as in Fig. 9, is shown in Fig. 10. As the analytical approach always overestimates the average relative velocity, also the the collision probability is slightly higher for the analytical method. The relative error is in any case small: for example, among the cases in Fig. 10, the case F(1000,90)-T(1000,0) has the largest relative error on the cumulative collision probability and it is equal to 9.71%. Therefore, the method is suitable to model, on the long term, different collision scenarios with an acceptable level of error.

VI. COLLISION SCENARIOS

Thanks to its limited computational time and its good accuracy, the method described in Sec. II can be applied to study the collision probability due to small fragments in many different scenarios. The method can be applied, for example, to study the impact of a breakup on different target spacecraft or to build, for each target spacecraft or for a whole set of targets, a *map* of collision probability is built by varying the inclination and the altitude of the simulated breakup[24].

Here, instead, the method is used to generate a *matrix of influence* among a set of targets. Ther targets used for the simulations are listed in Tab. 1: they were extracted from a list prepared by IFAC-CNR, ISTI-CNR and University of Southampton for a study sponsored by the European Space Agency[25]. The objects in Tab. 1 are the ten spacecraft with the largest collision probability and they are sorted by their semi-major axis.

The *influence matrix* wants to study the following situation: a small breakup caused by a non-catastrophic collision with one of the spacecraft in Tab. 1, generates a fragment cloud that can interfere with other spacecraft. Each spacecraft in Tab. 1 is treated as a potential target and its collision probability due to the fragment cloud is computed. This process is repeated scrolling through the whole list of spacecraft in Tab. 1 to obtain a picture of how each spacecraft affects the collision probability of the other ones.

ID	Target	h_p [km]	h_a [km]	i [deg]	Mass [kg]	Size [m]
1	ESA-3541	762.9208	764.3492	98.45	8110	8.96
2	ESA-253	790.9662	796.7038	85.00	4580	5.78
3	ESA-271	799.7443	806.9258	64.90	16800	7.11
4	ESA-3847	815.9959	818.8741	98.67	4090	6.91
5	ESA-4419	816.0959	818.9741	98.73	4090	6.91
6	ESA-3189	820.5950	823.4750	98.54	2730	5.74
7	ESA-3410	837.8654	855.2046	70.99	3200	6.33
8	ESA-3047	830.2175	863.4525	70.90	3220	6.23
9	ESA-3926	842.6304	855.6396	70.98	3200	6.33
10	ESA-3692	842.9113	863.1587	71.00	3200	6.33

Tab. 1: List of target spacecraft[25] for the collision probability analysis

VI.I. Influence matrix

Fig. 11 shows the resulting influence matrix for the spacecraft in Tab. 1 considering a fragmentation of 100 kJ and plotting the resulting collision probability after five years.

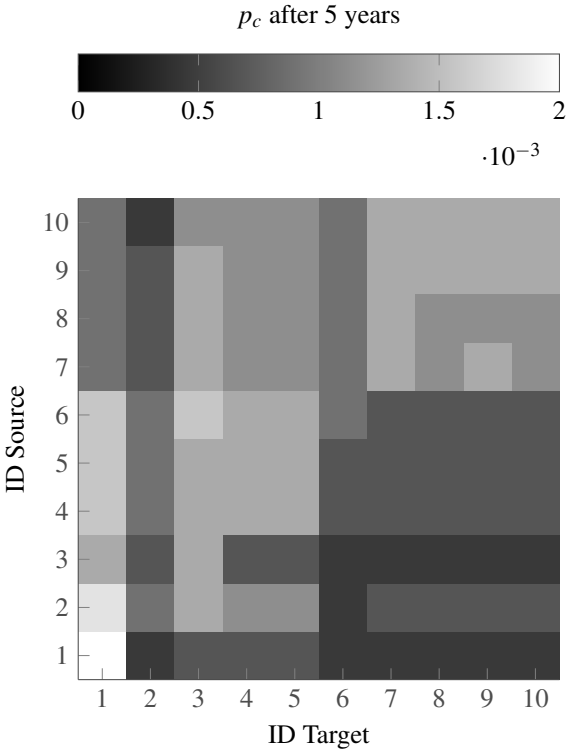

Fig. 11: Influence matrix for 10 target spacecraft.

Here it is important to specify that, as the proposed method is able to provide an analytical expression for the density only after the band is formed, the collision probability is computed starting from that moment. This means the collision probability is underestimated for satellites such as SC7-SC10 that have very similar orbit and that may start to interact before the band is formed. Future work will aim to estimate the collision probability also before the band formation.

From Fig. 11 it is possible to recognise that, as one can expect, the influence is very strong among satellites on similar orbits such as the already cited group SC7-SC10 and also SC4-SC5. The maximum influence is registered for SC1, which is in an much lower orbit than the other spacecraft and which has a much larger cross area (more than 250 m^2 compared to 100-160 m^2 for the other spacecraft, assuming a spherical shape). This also explains why it appears to be a *vulnerable* target for all the fragmentations originating from SC2-SC6. A similar behaviour is observed also for SC3, due, in this case, both to the low semi-major axis and the low inclination. In fact, SC3 has the lowest inclination among all the spacecraft in Tab. 1 and this means that it will be always inside the bands generated by the simulated breakups.

The sum of the collision probability for all the targets due to the same source can be instead used as an index of the spacecraft influence, as shown in Fig. 12.

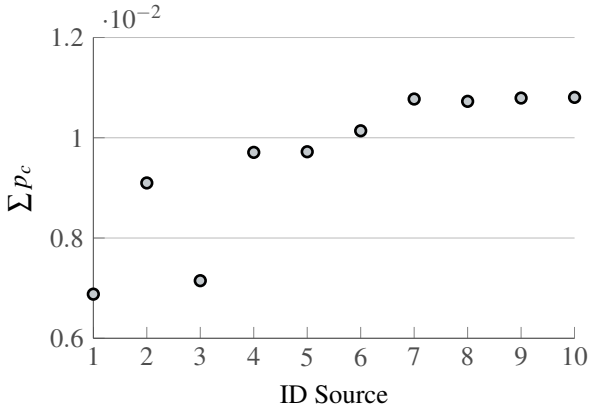

Fig. 12: Sum of the generated collision probability for the scenario in Fig. 11.

SC10 is the spacecraft with the largest impact on the total collision probability, with similar values for all the spacecraft in the group SC7-SC10. This result can be ex-

plained looking once more at the spacecraft parameters in Tab. 1. SC7-SC10 have large semi-major axis and large inclination, so the resulting fragment bands are crossed by all the spacecraft in the list; moreover, the interaction among the satellites in this group increases the total collision probability.

The computational time required to generate Fig. 11 is equal to 645 s on a PC with 8 CPUs at 3.40 GHz. The process is fully automatic and parallised, so the the number of spacecraft in the list can be extended to obtain a more complete picture of the mutual influence among what are considered the most critical objects in the debris population in LEO.

VII. CONCLUSION

Small debris fragments are often not included in the study of the evolution of the debris population even if they can still pose a relevant hazard to spacecraft in case of collision. The number of small fragments is too large to follow each object separately. This work discussed a method to treat them in terms of their resulting spatial density. Different approaches are possible to convert the information on the fragment position to a continuous density function. Two possible expressions for the spatial density were compared and the one from Kessler was chosen because of its better performance in the description of the peak in the fragment spatial distribution. Once the initial density profile was defined, its evolution with time under the effect of drag was obtained by applying the continuity equation, which allows deriving an explicit expression for the density as a function of time and distance. The dependence of the fragment density on the latitude was instead neglected as the focus was on the long term evolution of the cloud, whereas the latitude of a possible target spacecraft evolves on a much shorter time scale. The explicit expression for the density allows the method to provide a very fast estimation of the extension of the region of space affected by the fragmentation and of the resulting collision probability for a spacecraft in those region. For this reason, the proposed method can be applied to simulate many collision scenarios in a short time, enabling new analysis on the contribution of small fragments to the collision probability. In particular, here the method was applied to study the mutual influence among a list of spacecraft in the case they originate a fragment cloud as a result of a small breakup. The resulting matrix of collision probability can be useful to identify which objects, in case of fragmentations, are more likely to have a large impact on the global collision probability and are therefore critical items in the debris population.

ACKNOWLEDGEMENT

Francesca Letizia would like to thank the European Space Agency for the sponsorship that enabled her to participate in the IAC 2014. Camilla Colombo acknowledges the support received by the Marie Curie grant 302270 (SpaceDebECM - Space Debris Evolution, Collision risk, and Mitigation), within the 7th European Community Framework Programme. The authors acknowledge the use of the IRIDIS High Performance Computing Facility, and associated support services at the University of Southampton, in the completion of this work.

[1] V. Chobotov. *Orbital mechanics*. AIAA, Reston, 3rd edition, 2002. ISBN 1563475375.

[2] A. E. White and H. G. Lewis. The many futures of active debris removal. *Acta Astronautica*, 95:189–197, February 2014. doi: 10.1016/j.actaastro.2013.11.009.

[3] P. H. Krisko. The predicted growth of the low-Earth orbit space debris environment an assessment of future risk for spacecraft. *Proceedings of the Institution of Mechanical Engineers, Part G: Journal of Aerospace Engineering*, 221(6):975–985, January 2007. doi: 10.1243/09544100JAERO192.

[4] A. Rossi, A. Cordelli, and C. Pardini. Modelling the space debris evolution: Two new computer codes. *Advances in the Astronautical Sciences-Space Flight Mechanics*, pages 1–15, April 1995.

[5] C. R. McInnes. An analytical model for the catastrophic production of orbital debris. *ESA Journal*, 17(4):293–305, 1993.

[6] F. Letizia, C. Colombo, and H. G. Lewis. Analytical model for the propagation of small debris objects clouds after fragmentations. *Journal of Guidance, Control, and Dynamics*, 2014. [Accepted].

[7] N. L. Johnson and P. H. Krisko. NASA's new breakup model of EVOLVE 4.0. *Advances in Space Research*, 28 (9):1377–1384, 2001. doi: 10.1016/S0273-1177(01)00423-9.

[8] P. H. Krisko. Proper Implementation of the 1998 NASA Breakup Model. *Orbital Debris Quarterly News*, 15(4): 1–10, 2011.

[9] D. S. McKnight. A phased approach to collision hazard analysis. *Advances in Space Research*, 10(3-4):385–388, January 1990. doi: 10.1016/0273-1177(90)90374-9.

[10] R. Jehn. Dispersion of debris clouds from In-orbit fragmentation events. *ESA Journal*, 15(1):63–77, 1991.

[11] D. A. Vallado. *Fundamentals of astrodynamics and applications*. Springer, 4th edition, 2013. Pages 551–573, 619–688. ISBN: 978-1881883180.

[12] D. King-Hele. *Satellite orbits in an atmosphere: theory and application*. Blackie, Glasgow and London, 1987. ISBN 0216922526.

[13] J. Ashenberg. Formulas for the phase characteristics in the problem of low-Earth-orbital debris. *Journal of Spacecraft and Rockets*, 31(6):1044–1049, November 1994. doi: 10.2514/3.26556.

[14] F. Letizia, C. Colombo, and H. G. Lewis. Continuity equation method for debris cloud evolution. In *International workshop on Key Topics in Orbit Propagation Applied to Space Situational Awareness*, Logroño, April 2014.

[15] F. Letizia, C. Colombo, H. G. Lewis, and C. R. McInnes. Debris cloud evolution in Low Earth Orbit. In *International Astronautical Congress*, Beijing, September 2013. IAC-13.A6.P.12.

[16] H. Klinkrad. *Space Debris: Models and Risk Analysis*. Springer Praxis Books. Springer, 2006. ISBN 9783540376743. Pages 15,120.

[17] S.-Y. Su and D. Kessler. Contribution of explosion and future collision fragments to the orbital debris environment. *Advances in Space Research*, 5(2):25–34, January 1985. doi: 10.1016/0273-1177(85)90384-9.

[18] C. R. McInnes and C. Colombo. Wave-like patterns in an elliptical satellite ring. *Journal of Guidance, Control, and Dynamics*, 36(6):1767–1771, 2013. doi: 10.2514/1.55956.

[19] D. J. Kessler. Derivation of the collision probability between orbiting objects: the lifetimes of Jupiter's outer moons. *Icarus*, 48(1):39–48, October 1981. doi: 10.1016/0019-1035(81)90151-2.

[20] M. Sykes. Zodiacal dust bands: Their relation to asteroid families. *Icarus*, 9, 1990.

[21] E. J. Öpik. Collision probabilities with the planets and the distribution of interplanetary matter. *Proceedings of the Royal Irish Academy. Section A: Mathematical and Physical Sciences*, pages 165–199, 1951.

[22] D. Kessler. Collision probability at low altitudes resulting from elliptical orbits. *Advances in Space Research*, 10 (3):393–396, 1990.

[23] A. Jenkin and R. Gick. Dilution of disposal orbit collision risk for the medium Earth orbit constellations. Technical Report 8506, The Aerospace Corporation, Los Angeles, 2005.

[24] F. Letizia, C. Colombo, and H. G. Lewis. Small debris fragments contribution to collision probability for spacecraft in Low Earth Orbit. In *7th IAASS Conference*, Friedrichshafen, October 2014.

[25] A. Rossi, G. B. Valsecchi, L. Anselmo, C. Pardini, H. G. Lewis, and C. Colombo. Fragmentation consequence analysis for leo and geo orbits. In *GreenOps Workshop*, Noordwijk, November 2013. ESA AO 1/7121/12/F/MOS.